Applied Physics Letters

Identifying the local defect structure in $(Na_{0.5}K_{0.5})NbO_3$: 1 mol. % CuO lead-free ceramics by x-ray absorption spectra

Cite as: Appl. Phys. Lett. **114**, 092904 (2019); https://doi.org/10.1063/1.5088397
Submitted: 10 January 2019 . Accepted: 16 February 2019 . Published Online: 05 March 2019

Jian Fu, Ruzhong Zuo, He Qi, and Tingshan Chan

AIP Publishing

Applied Physics Letters ARTICLE scitation.org/journal/apl

Identifying the local defect structure in $(Na_{0.5}K_{0.5})NbO_3$: 1 mol. % CuO lead-free ceramics by x-ray absorption spectra

Cite as: Appl. Phys. Lett. **114**, 092904 (2019); doi: 10.1063/1.5088397
Submitted: 10 January 2019 · Accepted: 16 February 2019 ·
Published Online: 5 March 2019

View Online Export Citation CrossMark

Jian Fu,[1] Ruzhong Zuo,[1,a)] He Qi,[1] and Tingshan Chan[2]

AFFILIATIONS

[1]Institute of Electro Ceramics and Devices, School of Materials Science and Engineering, Hefei University of Technology, Hefei 230009, People's Republic of China
[2]National Synchrotron Radiation Research Center, 101 Hsin-Ann Road, Hsinchu Science Park, Hsinchu 30076, Taiwan

[a)]Email: rzzuo@hotmail.com

ABSTRACT

The local defect structure around dopant atoms in 1 mol. % CuO doped $(Na_{0.5}K_{0.5})NbO_3$ lead-free ceramics was investigated by means of x-ray absorption spectra as compared with the local structure around the host Nb site. The Cu *K*-edge and O *K*-edge x-ray absorption near-edge structure spectra demonstrate divalent Cu ions that occupy the octahedrally coordinated Nb sites and also reveal the existence of oxygen vacancy $V_O^{\cdot\cdot}$ in the nearest neighboring around the Cu atom evidently. Moreover, the Cu and Nb *K*-edge extended x-ray absorption fine structure clearly suggests that the oxygen vacancies should be located at two O22 sites with the two longest Cu-O22 bond lengths, thus producing trimeric bent $V_O^{\cdot\cdot}$-$Cu_{Nb}^{\prime\prime\prime}$-$V_O^{\cdot\cdot}$ defect complexes with a dipole moment P_D parallel to the spontaneous polarization P_s, instead of dimeric $Cu_{Nb}^{\prime\prime\prime}$-$V_O^{\cdot\cdot}$ and straight $V_O^{\cdot\cdot}$-$Cu_{Nb}^{\prime\prime\prime}$-$V_O^{\cdot\cdot}$ defect complexes. This kind of special defect structure is also different from that observed in conventional Pb-based perovskite ferroelectrics in which only dimeric $Cu_{Ti}^{\prime\prime}$-$V_O^{\cdot\cdot}$ defect dipoles were observed. Finally, the influence of the defect complexes on the macroscopic properties was specially discussed by taking into account the interaction between P_s and P_D.

$(Na_{0.5}K_{0.5})NbO_3$ (NKN) based lead-free ferroelectric ceramics have attracted much attention due to their relatively high Curie temperature and good piezoelectric properties. For high-power applications, their ferro/piezo-electric properties can be tailored by adding acceptor transition metal ions, which usually induce negatively charged defects (i.e., impurity defects) and positively charged defects (i.e., oxygen vacancy, $V_O^{\cdot\cdot}$). It has been well accepted that these defects are either isolated or form defect dipoles between impurities and oxygen vacancies.[1–3] For isolated defects, the impurity defect is far away from $V_O^{\cdot\cdot}$; thus, there is no strong interaction between them. As a result, $V_O^{\cdot\cdot}$ should be most mobile and tend to migrate within domain walls as an ionic charge barrier to compensate the polarization charges.[4–6] However, once the impurity defect and the $V_O^{\cdot\cdot}$ are close to each other, they tend to form the defect dipole. The first principles calculation has proposed that the defect complex should be more stable owing to its lower formation energy.[7–11] The defect complex is believed to cooperatively align along the direction of spontaneous polarization (P_s) and to act as the pinning centers to inhibit domain switching.

Despite the importance of defects, it is still not clear how exact the coordination sphere around the defect center is and how it influences the macroscopic ferro-/piezoelectric properties. The defect structure around the impurity ions, such as Cu^{2+}, Fe^{3+}, and Mn^{2+} in perovskite-structured ferroelectrics, was widely investigated using electron paramagnetic resonance (EPR) spectroscopy,[12–18] through which different charge compensation mechanisms between titanates and alkali niobates were found to result in diverse defect structures. However, EPR is only sensitive to paramagnetic ions with unoccupied electrons and thus shows a limitation under the condition that the valence state and local structure of the ions in the host center were changed after doping[19] because it cannot distinguish whether the defect structure or the local host structure induces the change of macroscopic properties. In addition, as far as alkaline niobates are concerned, only low-temperature EPR data in literature studies so far can be reviewed.[12,17] These data cannot precisely identify the actual local defect structure considering that NKN undergoes a successive polymorphic phase transition during heating/cooling. In contrast, the x-ray absorption fine structure (XAFS) measurement can directly probe

the local coordination environment around the absorption atom and has been widely used for titanates and ferrites[19–24] but rarely reported in niobates.[25,26]

In this paper, the valence state and the site occupation of the Cu atoms in 1 mol. % CuO doped (NKNC) were investigated by means of extended XAFS (EXAFS) and near-edge XAFS (x-ray absorption near-edge structure, XANES) spectra. The results indicate that divalent Cu ions should be incorporated at the octahedrally coordinated Nb sites, forming the bent $V_O^{\cdot\cdot}$-$Cu_{Nb}^{\prime\prime\prime}$-$V_O^{\cdot\cdot}$ defect complex with a net dipole moment P_D parallel to P_s. The influence of the defect complex on the macroscopic performances was also discussed by taking into account the interaction between P_s and P_D.

Undoped NKN and NKNC ceramics were fabricated by a conventional solid state route, as described elsewhere.[3] The crystalline structure was examined using an x-ray diffractometer (XRD, D/MAX2500VL/PC, Rigaku, Japan) using Cu Kα radiation. The structure refinement was carried out using GSAS software.[27] Two samples can be well described by orthorhombic phase with Amm2 symmetry, and no obvious lattice parameters change can be observed (see Fig. S1 and Table S1). XANES and EXAFS spectra were recorded with a beamline 01C1 at the National Synchrotron Radiation Research Center (NSRRC), Hsinchu, Taiwan. The Cu *K*-edge absorption spectra were recorded by the fluorescence yield mode using a Lytl1 detector. The Nb *K*-edge absorption spectra were recorded in the transmission mode. The k^3-weighted magnitudes in the R space were derived from the Fourier transformation (FT) over the k range of 2–14.5 $Å^{-1}$ for both the Nb *K*- and Cu *K*-edges by using Athena software. Scattering paths were determined by the FEFF 6 code.[28] Fitting was performed in the R range 0.8–2.5 Å using the Artemis program of the IFEFFIT package based on the multiple scattering theory. The XANES spectrum of O *K*-edge was measured at a beam line 20 A high-energy spherical grating monochromator (HSGM) at the NSRRC, Hsinchu, Taiwan. The spectra were recorded in the total-electron-yield mode and normalized for comparison. The polarization versus electric field (P-E) hysteresis loops were measured at 10 Hz using a ferroelectric testing system (Precision Multiferroic, Radiant Technologies Inc., Albuquerque, NM). The Cu 2p binding energy was recorded by X-ray photoelectron spectroscopy (XPS, PHI 5802, Physical Electronic Inc., USA).

The Cu *K*-edge XANES spectra of the NKNC sample together with the reference samples of Cu_2O and CuO are shown in Fig. 1. Two features labeled as A and B corresponding to the transition from 1s states to axial and planar 4p states, respectively,[29,30] can be observed in all samples. It is found that the peak positions of features A and B show a distinct shift towards high energies as the valence of Cu ions increases because the core level becomes more tightly bound in higher valence states. As shown in Fig. 1, the energy shifts of features A and B from Cu_2O to CuO are 3.9 eV and 1.8 eV, respectively, which were believed to be associated with the valence state change from Cu^{1+} to Cu^{2+}.[31,32] Very interestingly, the peaks A and B in the XANES spectrum of NKNC are located at the same positions as the corresponding peaks in the spectrum of CuO, indicating that only Cu^{2+} ions should exist in the NKNC sample, instead of any Cu^{1+} or the mixed valences. The XPS result also indicates that no mixed valence states can be observed (see Fig. S2). In addition, it can be seen from the inset of Fig. 1 that the electronic structure around Cu atoms is remarkably similar in both CuO and NKNC, but different between Cu_2O and NKNC,

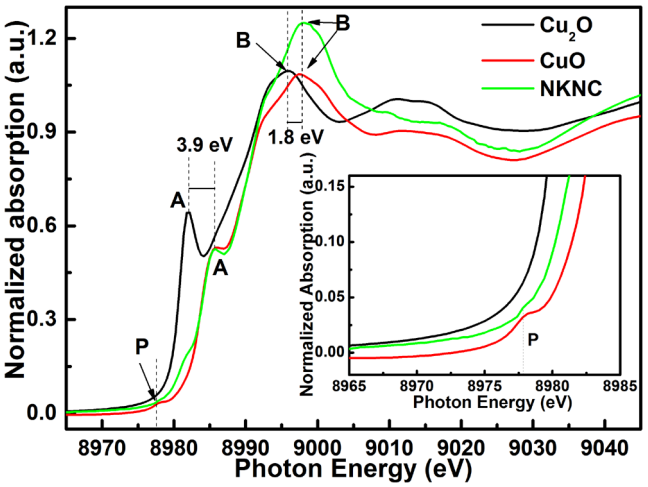

FIG. 1. Cu K-edge XANES spectra of the NKNC sample in comparison with the reference samples of Cu_2O and CuO. The inset shows the pre-edge structure of the corresponding samples.

possibly because a broad shoulder (denoted as P) can be observed in both CuO and NKNC samples, rather than in the monovalent Cu compounds (i.e., Cu_2O).

Figure 2(a) shows the O *K*-edge XANES spectra of NKN and NKNC samples. Four characteristic peaks (marked by A1–D1) associated with the transition from the O 1s core states to the unoccupied O 2p states can be identified. According to the literature,[33,34] the strong peaks A1 and C1 observed in the NKN sample are attributed to the hybridization between the Nb 4d state and the O 2p state. By comparison, B1 and D1 peaks are extremely weak because of the ionic K/Na-O bond. As a result, the polarization contribution of A-site ions should be extremely low, and consequently, the A-site displacement can be neglected in the present study. It is of importance to note that the intensity of A1 and C1 peaks shows an obvious increase after CuO doping compared with the intensity of B1 and D1 peaks, possibly because Cu^{2+} should preferentially occupy the octahedrally coordinated Nb site as an acceptor dopant rather than the Na/K site. Figure 2(b) presents the Nb *K*-edge XANES of the NKN and NKNC samples in comparison with the Cu *K*-edge XANES of the NKNC sample. There exist obvious differences in main peaks at the white line between the Nb *K*-edge and the Cu *K*-edge due to the different d-final states between them. In addition, a weak post-edge peak denoted as L at ~9010 eV can be observed in the Cu *K*-edge spectrum for the NKNC sample but is absent in Nb *K*-edge spectra for both NKN and NKNC samples. This result should be due to the removal of the oxygen in the nearest neighboring around the Cu atom in NKNC, i.e., the formation of $V_O^{\cdot\cdot}$ around the absorption Cu atom, rather than the different atomic-like final states, since the feature L is also absent in the Cu K-edge spectra of CuO and Cu_2O as shown in Fig. 1.

The FT magnitudes of the k^3 weighted Nb *K*-edge and Cu *K*-edge EXAFS are shown in Fig. 3(a). The magnitude of FT peaks is correlated with the coordination number around the absorption atoms and the Debye-Waller factor, while the position of FT peaks depends on the interatomic distance. It can be seen that no obvious local structure change occurs around the Nb atoms after CuO doping. The

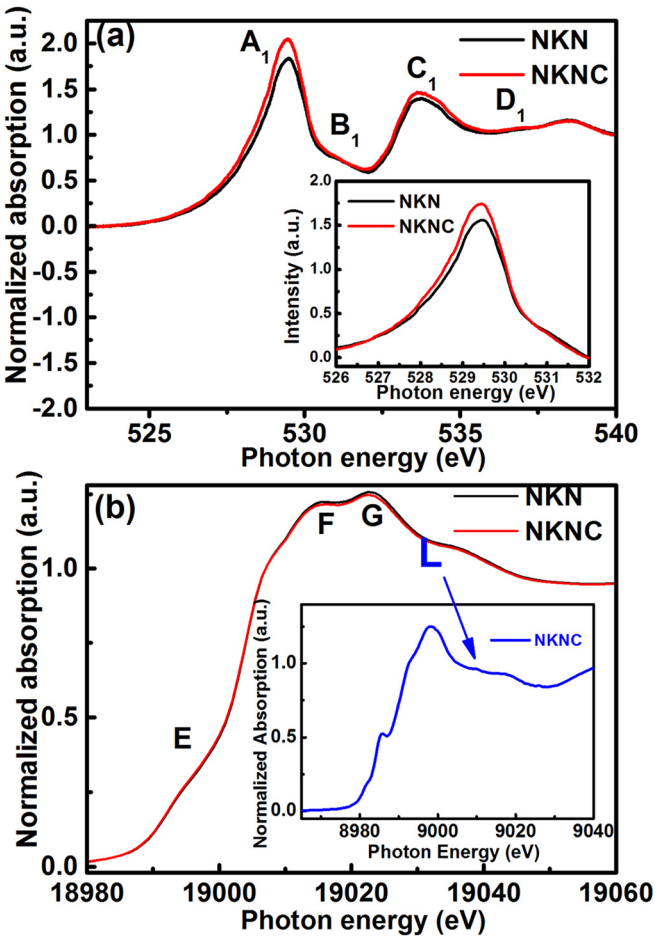

FIG. 2. (a) O K-edge XANES spectra and (b) Nb K-edge XANES spectra for the NKN and NKNC sample. The inset in (a) shows the magnified near-edge feature after background subtraction of O K-edge XANES spectra and the inset in (b) shows the Cu K-edge XANES spectra of the NKNC sample.

preferred site occupation of Cu atoms can be also determined. Suppose that Cu atoms enter the A site, the first main peak in the Cu *K*-edge EXAFS spectrum should be expected to lie roughly at 2 Å (no phase correction)[34,35] due to the twelve nearest oxygen in the O_{12} cage, in which each oxygen atom should be at the center of the face diagonal. However, the first main peak in the Cu *K*-edge EXAFS spectrum is found to be located at ~1.5 Å (no phase correction), confirming that Cu atoms occupy the B-site similar to that of Nb atoms. This should be attributed to their similar radii [coordination number (CN) = 6, $R_{Cu} = 0.73$ Å, $R_{Nb} = 0.64$ Å].[36] It is noteworthy that only a single peak appears in the R range of 1–2 Å for the Cu *K*-edge spectrum. This is different from the double-peak structure in Nb *K*-edge spectra, possibly because of the existence of $V_{\ddot{O}}$ around Cu atoms. In addition, it can be found that the FT magnitude data for Cu *K*-edge EXAFS spectrum are dominated by the first oxygen and second alkali coordination shells, while only small contributions in high R space (>3 Å) can be observed. This is different from the Nb *K*-edge EXAFS spectra, indicating that the long-range ordering of Cu atoms is absent in the NKN

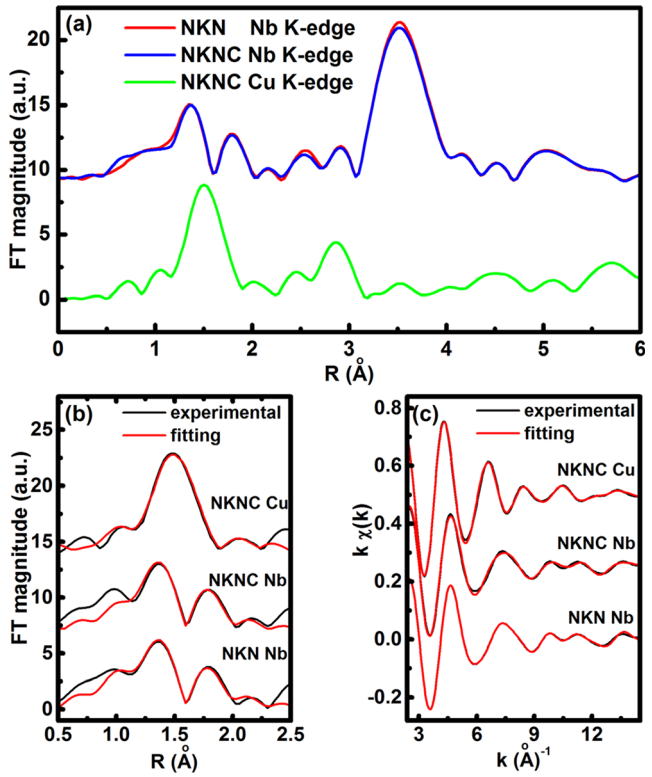

FIG. 3. FT magnitudes of the k^3 weighted (a) Nb K-edge EXAFS spectra for NKN and NKNC samples and (b) the comparison between the experimental FT EXAFS spectra (dots) and fitting results (lines) of the nearest neighboring and (c) the comparison between filtered experimental (dots) and fitting (lines) EXAFS spectra.

matrix. Figures 3(b) and 3(c) show the fits in the first coordination corresponding to the nearest oxygen neighbors. The experimental EXAFS oscillations and filtered EXAFS spectra are in good agreement with the fitted spectra except for the EXAFS oscillations in the R range lower than 1 Å, which is affected by the background subtraction procedure and thus not considered in the fitting process. The fitting results and the corresponding parameters are listed in Table S2.

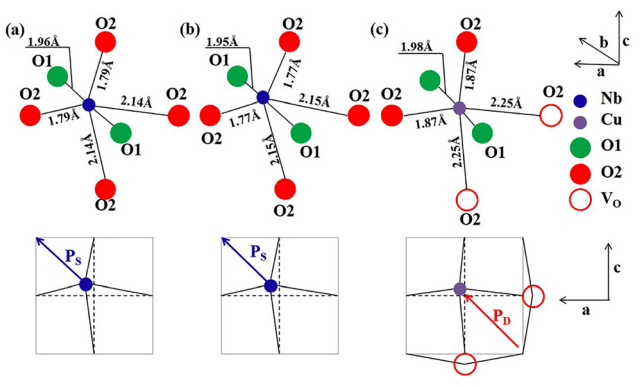

FIG. 4. The sketch of the oxygen octahedron around the Nb atom for (a) NKN and (b) NKNC samples and (c) around the Cu atom for the NKNC sample.

Figure 4 shows the schematic illustration of the first oxygen shell around the Nb/Cu atom according to the results listed in Table S2. Compared with the Nb atoms, the Cu defect center is found to move away from the oxygen at O21 and O1 sites, meaning that the relative displacement of the Cu atom with respect to the nearest oxygen neighbors at O21 and O1 sites decreases.[7,37] The atomic position relaxation favors the Cu atom to decouple the bond with oxygen but tends to form defect dipoles due to the electrostatic Coulomb interaction. In addition, a distinct $V_O^{\cdot\cdot}$ relaxation is also observed as it moves far away from the Cu atom. This should be because of a relatively small electrostatic Coulomb interaction between Cu atoms and oxygen vacancies, compared with the interaction between Nb atoms and oxygen atoms.[26] The result shows good agreement with the density functional theory (DFT) calculations,[8,11] in which $V_O^{\cdot\cdot}$ was found to repel the nearest dopant atoms. On the other hand, the fitted coordination number and oxygen vacancy site suggested that these oxygen vacancies tend to form trimeric bent $V_O^{\cdot\cdot}$-$Cu_{Nb}^{'''}$-$V_O^{\cdot\cdot}$ defect complexes with a net P_D parallel to the P_s [Fig. 4(c)], instead of dimeric $Cu_{Nb}^{'''}$-$V_O^{\cdot\cdot}$ or straight $V_O^{\cdot\cdot}$-$Cu_{Nb}^{'''}$-$V_O^{\cdot\cdot}$ defect complexes. This phenomenon is different from that of Cu doped $PbTiO_3$ (PT), in which only dimeric $Cu_{Ti}^{''}$-$V_O^{\cdot\cdot}$ defect dipoles (anti)parallel or perpendicular to c ([001]) axis were observed.[8,9] In this case, the negatively charged acceptor center $Cu_{Ti}^{''}$ can be well compensated by one $V_O^{\cdot\cdot}$, which, however, is not suitable for the NKNC sample. Instead, the negatively charged $Cu_{Nb}^{'''}$ center in NKNC must be either partially compensated by one $V_O^{\cdot\cdot}$ or overcompensated by two $V_O^{\cdot\cdot}$. In addition, the observed $V_O^{\cdot\cdot}$-$Cu_{Nb}^{'''}$-$V_O^{\cdot\cdot}$ defect complex is bent and thus cannot form the Cu-O-Cu chain. As a result, the antipolar domains that were observed in PT[38] may not be detected in the present study. The defect structure in NKNC is also found to be different from the $Cu_{Nb}^{'''}$-$V_O^{\cdot\cdot}$ and/or straight $V_O^{\cdot\cdot}$-$Cu_{Nb}^{'''}$-$V_O^{\cdot\cdot}$ as determined by EPR.[12,39] The latter might be due to the low dopant concentration and low measuring temperatures.

It can be seen from Fig. 4 that the Nb atom in both NKN and NKNC shows an obvious off-center shift along the diagonal of the ac plane, corresponding to the P_s along the [101] direction. Polarization switching will occur only if the energy barrier between different P_s directions can be overcome. As bent $V_O^{\cdot\cdot}$-$Cu_{Nb}^{'''}$-$V_O^{\cdot\cdot}$ defect complexes are present, the energy barriers between P_s directions will become nonequivalent because the removal of the oxygen at O22 sites breaks the perfect orthorhombic symmetry. On the one hand, the P_D between two adjacent $Cu_{Nb}^{'''}$-$V_O^{\cdot\cdot}$ defect dipoles is parallel to the P_s [Fig. 4(c)], so their interactions tend to stabilize the ferroelectric polarization along the direction parallel to the orientation of the defect dipole. That is to say, the polarization along the [101] direction becomes more stable than along other ⟨101⟩ directions, and the energy barrier between [101] and other ⟨101⟩ directions thus increases. On the other hand, the theoretical calculation proposed that the rotation of the defect dipole should be much more difficult than the polarization switching since the former involved the migration of oxygen within the lattice.[11] This means that the defect dipole tends to remain in its original direction during polarization switching. Once the polarization switching occurs, the orientation of P_s is not collinear with the direction of P_D but shows obvious included angles [$\angle(P_s, P_D) \approx 60°$, 90°, 120°, and 180°], depending on the initial directions of P_s and P_D with respect to the direction of the external electric field. This process would accompany an increase in the electrostatic energy and the elastic energy. These increased energy barriers would be responsible for the obvious hardening effect in NKNC (see Fig. S3 and Table S3).

Although only trimeric $V_O^{\cdot\cdot}$-$Cu_{Nb}^{'''}$-$V_O^{\cdot\cdot}$ defect complex is observed in the current study, other defect configurations such as $Cu_{Nb}^{'''}$-$V_O^{\cdot\cdot}$ and straight $V_O^{\cdot\cdot}$-$Cu_{Nb}^{'''}$-$V_O^{\cdot\cdot}$ should not be ruled out, because both the processing condition and the dopant concentration significantly affect the site occupation and the defect structure.[12,26] However, in the case of the $Cu_{Nb}^{'''}$-$V_O^{\cdot\cdot}$ defect complex, P_D should be along one of the ⟨001⟩ directions rather than ⟨101⟩ directions, leading to the increase in the electrostatic energy. As a result, the coupling between P_s and P_D should be relatively weak, compared to the case in the bent $V_O^{\cdot\cdot}$-$Cu_{Nb}^{'''}$-$V_O^{\cdot\cdot}$ defect complex. Although no P_D exists in the case of straight $V_O^{\cdot\cdot}$-$Cu_{Nb}^{'''}$-$V_O^{\cdot\cdot}$ defect complex, it can result in an additional elastic energy. By comparison, both the elastic strain energy and the electrostatic energy will be minimized in the case of the bent $V_O^{\cdot\cdot}$-$Cu_{Nb}^{'''}$-$V_O^{\cdot\cdot}$ defect complex since the angle between P_s and P_D is the smallest. These results suggested that the binding energy of bent $V_O^{\cdot\cdot}$-$Cu_{Nb}^{'''}$-$V_O^{\cdot\cdot}$ defect dipoles should be the lowest, consistent with the DFT calculation.[11] Therefore, only a moderate hardening effect would be expected as if only $Cu_{Nb}^{'''}$-$V_O^{\cdot\cdot}$ or straight $V_O^{\cdot\cdot}$-$Cu_{Nb}^{'''}$-$V_O^{\cdot\cdot}$ defect complex existed, as in the case of 0.25 mol. % Cu doped NKN.[12] By comparison, it can be seen that an obvious hardening effect with large Q_m as high as 1500 can be observed in the present study (See Table S3). Lin *et al.* proposed that the hardening effect is remarkable only when the Cu concentration was beyond 0.5 mol. %.[40] These results further indicate that the Cu dopant content, oxygen vacancy concentration, and defect structure should be closely correlated. A detailed defect structure as a function of Cu^{2+} concentration needs to be constructed in future by means of x-ray absorption spectroscopy.

In summary, a detailed study on the local structure of NKN and NKNC lead-free ceramics was performed by means of x-ray absorption spectra. This study reveals that only divalent Cu ions exist and enter the octahedrally coordinated Nb site, resulting in the formation of $V_O^{\cdot\cdot}$. In particular, these oxygen vacancies are identified to lie at two O22 sites in the nearest oxygen neighboring around Cu ions. It is believed that trimeric bent $V_O^{\cdot\cdot}$-$Cu_{Nb}^{'''}$-$V_O^{\cdot\cdot}$ defect complexes are formed in the current study, instead of dimeric $Cu_{Nb}^{'''}$-$V_O^{\cdot\cdot}$ or straight $V_O^{\cdot\cdot}$-$Cu_{Nb}^{'''}$-$V_O^{\cdot\cdot}$ defect complexes. This kind of special defect structure is also different from that observed in conventional Pb-based perovskite compositions. An obvious ferroelectric hardening effect in NKNC was well interpreted in terms of the energy barrier between different P_s and the elastic and electrostatic energy owing to the coupling between P_s and P_D.

See supplementary material for the experimental supplement of the EXAFS measurement, XRD, XPS, and EXAFS fitting results, and various electrical properties.

This work was supported by the National Natural Science Foundation of China (Grants No. U1432113, 51402079, and 51332002).

REFERENCES

[1]D. M. Lin, K. W. Kwok, and H. L. W. Chan, Appl. Phys. Lett. **90**, 232903 (2007).
[2]F. Azough, M. Wegrzyn, R. Freer, S. Sharma, and D. Hall, J. Eur. Ceram. Soc. **31**, 569 (2011).
[3]J. Fu and R. Z. Zuo, J. Appl. Phys. **112**, 104114 (2012).
[4]D. M. Smyth, Annu. Rev. Mater. Sci. **15**, 329 (1985).
[5]P. V. Lambeck and G. H. Jonker, J. Phys. Chem. Solids **47**, 453 (1986).
[6]L. He and D. Vanderbilt, Phys. Rev. B **68**, 134103 (2003).

[7]H. Meštric, R.-A. Eichel, T. Kloss, K.-P. Dinse, S. Laubach, S. Laubach, P. C. Schmidt, K. A. Schönau, M. Knapp, and H. Ehrenberg, Phys. Rev. B **71**, 134109 (2005).
[8]P. Erhart, R.-A. Eichel, P. Träskelin, and K. Albe, Phys. Rev. B **76**, 174116 (2007).
[9]P. Erhart, P. Träskelin, and K. Albe, Phys. Rev. B **88**, 024107 (2013).
[10]A. Chandrasekaran, D. Damjanovic, N. Setter, and N. Marzari, Phys. Rev. B **88**, 214116 (2013).
[11]S. Körbel and C. Elsässer, Phys. Rev. B **88**, 214114 (2013).
[12]R.-A. Eichel, E. Erünal, P. Jakes, S. Körbel, C. Elsässer, H. Kungl, J. Acker, and M. J. Hoffmann, Appl. Phys. Lett. **102**, 242908 (2013).
[13]E. Aksel, E. Erdem, P. Jakes, J. L. Jones, and R.-A. Eichel, Appl. Phys. Lett. **97**, 012903 (2010).
[14]W. L. Warren, D. Dimos, G. E. Pike, K. Vanheusden, and R. Ramesh, Appl. Phys. Lett. **67**, 1689 (1995).
[15]R.-A. Eichel, P. Erhart, P. Träskelin, K. Albe, H. Kungl, and M. J. Hoffmann, Phys. Rev. Lett. **100**, 095504 (2008).
[16]D. J. Keeble, M. Loyo-Menoyo, Z. I. Y. Booq, R. R. Garipov, V. V. Eremkin, and V. Smotrakov, Phys. Rev. B **80**, 014101 (2009).
[17]E. Erünal, P. Jakes, S. Körbel, J. Acker, H. Kungl, C. Elsässer, M. J. Hoffmann, and R.-A. Eichel, Phys. Rev. B **84**, 184113 (2011).
[18]R. A. Maier, T. A. Pomorski, P. M. Lenahan, and C. A. Randall, J. Appl. Phys. **118**, 164102 (2015).
[19]Y. Yoneda, Y. Kitanaka, Y. Noguchi, and M. Miyayama, Phys. Rev. B **86**, 184112 (2012).
[20]I. Levin, V. Krayzman, J. C. Woicik, A. Tkach, and P. M. Vilarinho, Appl. Phys. Lett. **96**, 052904 (2010).
[21]I. A. Sluchinskaya, A. I. Lebedev, and A. Erko, J. Appl. Phys. **112**, 024103 (2012).
[22]E. Blokhin, E. Kotomin, A. Kuzmin, J. Purans, R. Evarestov, and J. Maier, Appl. Phys. Lett. **102**, 112913 (2013).
[23]N. Ishimatsu, T. Watanabe, K. Oka, M. Azuma, M. Mizumaki, K. Nitta, T. Ina, and N. Kawamura, Phys. Rev. B **92**, 054108 (2015).
[24]J. Jutimoosik, S. Hunpratub, S. Maensiri, S. Rujirawat, and R. Yimnirun, J. Appl. Phys. **116**, 104105 (2014).
[25]T. Vitova, J. Hormes, K. Peithmann, and T. Woike, Phys. Rev. B **77**, 144103 (2008).
[26]S. Körbel, P. Marton, and C. Elsässer, Phys. Rev. B **81**, 174115 (2010).
[27]A. C. Larson and R. B. Von Dreele, *General Structural Analysis System (GSAS)* (LANSCE, Los Alamos, New Mexico, 1994).
[28]B. Ravel and M. Newville, J. Synchrotron Radiat. **12**, 537 (2005).
[29]N. Kosugi, Y. Tokura, H. Takagi, and S. Uchida, Phys. Rev. B **41**, 131 (1990).
[30]J.-H. Choy, D.-K. Kim, S.-H. Hwang, and G. Demazeau, Phys. Rev. B **50**, 16631 (1994).
[31]E. E. Alp, G. K. Shenoy, D. G. Hinks, D. W. Capone II, L. Soderholm, H.-B. Schuttler, J. Guo, D. E. Ellis, P. A. Montano, and M. Ramanathan, Phys. Rev. B **35**, 7199 (1987).
[32]F. W. Lytle, R. B. Greegor, and A. J. Panson, Phys. Rev. B **37**, 1550 (1988).
[33]J. C. Jan, H. M. Tsai, C. W. Pao, J. W. Chiou, K. Asokan, K. P. Krishna, W. F. Pong, Y. H. Tang, M.-H. Tsai, S. Y. Kuo, and W. F. Hsieh, Appl. Phys. Lett. **87**, 012103 (2005).
[34]V. R. Mastelaro, H. R. Favarim, A. Mesquita, A. Michalowicz, J. Moscovici, and J. A. Eiras, Acta Mater. **84**, 164 (2015).
[35]B. Cherdhirunkorn, M. F. Smith, S. Limpijumnong, and D. A. Hall, Ceram. Int. **34**, 727 (2008).
[36]R. D. Shannon, Acta Crystallogr. A **32**, 751 (1976).
[37]S. Pöykkö and D. J. Chadi, Phys. Rev. Lett. **83**, 1231 (1999).
[38]C. H. Park and D. J. Chadi, Phys. Rev. B **57**, R13961 (1998).
[39]R. A. Eichel, E. Erünal, M. D. Drahus, D. M. Smyth, J. van Tol, J. Acker, H. Kungl, and M. J. Hoffmann, Phys. Chem. Chem. Phys. **11**, 8698 (2009).
[40]D. M. Lin, K. W. Kwok, and H. L. W. Chan, J. Phys. D: Appl. Phys. **41**, 045401 (2008).